Journal of Power Sources 273 (2015) 89–95

Contents lists available at ScienceDirect

Journal of Power Sources

journal homepage: www.elsevier.com/locate/jpowsour

Fabrication of thin yttria-stabilized-zirconia dense electrolyte layers by inkjet printing for high performing solid oxide fuel cells

Vincenzo Esposito*, Christophe Gadea, Johan Hjelm, Debora Marani, Qiang Hu, Karsten Agersted, Severine Ramousse, Søren Højgaard Jensen

DTU Energy Conversion and Storage, Technical University of Denmark, Risø Campus, Frederiksborgvej 399, DK-4000 Roskilde, Denmark

HIGHLIGHTS

- A gas-tight electrolyte of 1.2 μm for SOFC is made by a low-cost inkjet printer.
- Thin layers are deposited by colloidal inks with nanometric powders.
- Multiple printing on a flexible substrate achieves the continuity in the printing.

ARTICLE INFO

Article history:
Received 24 July 2014
Received in revised form
5 September 2014
Accepted 11 September 2014
Available online 19 September 2014

Keywords:
SOFC
Inkjet printing
YSZ
Colloidal suspension

ABSTRACT

In this work, we present how a low-cost HP Deskjet 1000 inkjet printer was used to fabricate a 1.2 μm thin, dense and gas tight 16 cm^2 solid oxide fuel cells (SOFC) electrolyte. The electrolyte was printed using an ink made of highly diluted (<4 vol.%) nanometric yttria stabilized zirconia (YSZ) powders (50 nm in size) in an aqueous medium. The ink was designed to be a highly dispersed, long term stable colloidal suspension, with optimal printability characteristics. The electrolyte was made by a multiple printing procedure, which ensures coverage of the several flaws occurring in a single printing pass. Together with an optimized sintering procedure this resulted in good adhesion and densification of the electrolyte. The SOFC exhibited a close-to-theoretical open circuit voltage and a remarkable peak power density above 1.5 W cm^{-2} at 800 °C.

1. Introduction

Additive manufacturing methods are of great importance in modern industry and inkjet printing of inorganic materials by use of colloidal suspensions as inks, has recently been spreading in several key technologies such as electronics [1], sensors [2], energy devices [3–6] and biomedical applications [7,8]. Despite that inkjet printing is usually considered a relatively low throughput fabrication method compared to other printing methods, it presents unique advantages in terms of customizable shapes and for printing of functional layers. Moreover, it is ideal for the fabrication of multi-component 2D and 3D architectures, which are formed additively drop by drop and layer by layer [9]. A technological domain in which these features are highly desirable is the solid oxide fuel cell (SOFC). This is especially relevant for the planar SOFC design, where the multi-material multilayers used in the components are well-interconnected and have different microstructural features [10–12]. Moreover, inkjet printing is ideal for the deposition of layers of about 1 μm in thickness [13] and this thickness range is valuable for the fabrication of SOFC electrolytes [14]. Among the different inkjet printing methods, Drop on Demand (DoD) printing by piezoelectric- or thermal-inkjet printing, has been used to fabricate SOFCs and SOFC components [10,15,16]. This is of great commercial interest due to the low-cost and high availability of such equipment on the market. Moreover, the different materials are prepared by simple chemistry and conventional powder technology methods, where the inks are stabilized in water-/alcohol-based suspensions [13].

In a typical planar SOFC, the electrolyte is made of 8 mol.% yttria-stabilized zirconia (8YSZ) [17–19]deposited on a tape casted NiO/8YSZ electrode layer on top of a NiO/3YSZ support layer [20].

* Corresponding author. Tel.: +45 46 77 56 37; fax: +45 46 77 58 00.
E-mail address: vies@dtu.dk (V. Esposito).

http://dx.doi.org/10.1016/j.jpowsour.2014.09.085
0378-7753/

Upon printing the electrolyte, the electrode and the support layer can be either a green material (i.e. the ceramic electrode shaped by the organic binder before the firing) or a consolidated pre-sintered NiO/YSZ substrate. After the printing, a sintering step at high temperatures, usually above 1200 °C [21], is required to obtain a dense and consolidated YSZ electrolyte layer.

High density of the electrolyte is a critical factor for the SOFC operation. The presence of flaws, pinholes or other defects can drastically reduce performance of the SOFC due to leaking of the fuel/oxidant gases through the electrolyte to the electrodes or by increasing resistance to oxygen ion diffusion in the electrolyte.

Several studies described the deposition of thin YSZ layers for SOFC anode layers using laboratory or commercial DoD printers [10–12]. Although these studies show that electrolytes and other components can be manufactured by inkjet printing, only a few studies report SOFCs with functional electrolytes with thicknesses of about 1 μm. Early promising results were obtained by Sukeshini and Cummins, who printed a YSZ electrolyte of about 10 μm by multiple printing (up to 12 layer-over-layer depositions) in a fully inkjet-printed SOFC [12]. In this and in other cases, multiple printings were necessary to seal the electrolyte to achieve acceptable performance and leak tightness of the cells. The importance of multiple printing was also recognized by Tomov et al. who deposited a 6 μm thick electrolyte by multiple printing (up to 10 printed layers) [10]. Recently, Li et al. successfully demonstrated that a 1.5 μm YSZ electrolyte layer for a SOFC could be printed by a single-layer deposition of ink containing nanoparticles in large agglomerates (between 0.2 and 5.5 μm) using a low-cost printer [16]. However, the resulting SOFC exhibited low power density and a low open circuit voltage indicating a leaky electrolyte.

In this work, we describe the manufacturing process of a printed and densified thin 8YSZ electrolyte of about 1 micron thickness and the subsequent electrochemical test results of a full anode-supported cell with this electrolyte. The electrolyte was printed onto a 9 × 9 cm^2 green layer of NiO/8YSZ anode using a modified low-cost DoD thermal printer, starting by diluted inks of nano-sized 8YSZ particles in water based suspension. To the best of our knowledge, this is the cells with the largest area inkjet-printed electrolyte reported so far.

2. Experimental

2.1. Ink preparation

Commercially available 8YSZ (8 mol.% yttria, TOSOH) nanometric powder was used for the fabrication of the electrolyte by inkjet printing. A water based ink was formulated by suspending the powders in a mix of 80 wt.% water and 20 wt.% ethanol. The powders were added to the liquid medium at two concentrations: 3.7 vol.% (concentrated ink) and 0.9 vol.% (dilute ink) of YSZ. Polyvinylpyrrolidone (PVP), dissolved in 53% weight ratio in pure ethanol, was used as dispersant and added into the YSZ suspension at ca. 8 mg m^{-2} of solid surface area. All constituents were then milled in a rotational mill in a PET flask at 100 rpm using zirconia milling balls for 10 days. The particle size distribution after mixing was measured using a laser particle size analyzer (Beckman Coulter, LS 13320).

2.2. Ink characterization

Rheological measurements were carried out with an Anton Paar rheometer (MCR 302), in rotational mode and at a constant temperature of 21 °C. A plate–plate measuring system was used with a diameter of 50 mm (PP50) and a gap distance of 0.6 mm. The experiments were performed using three steps of pre-treatment: the first one at 0.1 s^{-1} for 1 min followed by 1 min at rest (0 s^{-1} shear rate), and the third one at 10 s^{-1} for 1 min. Flow curve measurements were conducted in step mode using 60 steps with a waiting time of 10 s. The shear rates investigated range from 10 s^{-1} up to 1000 s^{-1}, in the up ramp, and from 1000 s^{-1} to 10 s^{-1} in the down ramp.

Ink surface tension was measured using a bubble pressure tensiometer (BP 50, Krüss).

The printability of the inks was assessed by determining their *Z*, Weber (*We*), and Reynolds (*Re*) numbers, graphically combined as report by Derby [28,31], and defined as:

$$We = \frac{v^2 \rho a}{\sigma} \quad (1)$$

$$Re = \frac{v \rho a}{\eta} \quad (2)$$

$$Z = \frac{1}{Oh} = \frac{\sqrt{\sigma . \rho . a}}{\eta} \quad (3)$$

where v is the drop velocity, η is the ink viscosity, σ is the surface tension, ρ is the density, and a is the characteristic length [28]. The parameter a is typically taken as the diameter of the printing nozzles (20 μm). The *We* and *Re* numbers were calculated within the typical reported range of values for the drop velocity (1–30 m s^{-1}) [22].

2.3. SOFC fabrication

2.3.1. NiO/YSZ substrates

The substrates used for the tested SOFC consisted in thin NiO/YSZ functional anode layer deposited onto a thicker NiO/YSZ anode support. The ratio between Ni and YSZ was 40/60 vol.% both for the support layer and the active electrode layer [23]. ZrO_2 stabilized with 8 mol.% Y_2O_3 was used for the anode layer while ZrO_2 stabilized with 3 mol.% Y_2O_3 was used for the support layer. The layer produced by tape-casting and co-laminated as green materials at ca. 150 °C [23]. The substrates had a 10–15 μm thick anode of Ni/YSZ cermet laminated to a~300 μm thick Ni/YSZ support layer.

2.3.2. Electrolyte layer deposition by inkjet printing

A commercially available printer (HP Deskjet 1000) was used as a printing unit. The printer was modified to allow a range of different print head/substrate distances and to print on thick and stiff substrates. A compatible cartridge (HP 301 black) providing a 600 × 300 dpi resolution was cleaned to remove the original black ink and used to print the ceramic ink. The YSZ inks were inserted into the cartridge manually using syringes. Two printing procedures were used for the printing:

- “Single Droplets” printing (SD), consisting in printing isolated droplets using a square-chess-like pattern, it was aimed to control the quality of the single droplet or presence of flaws in the DoD printing;
- “Continuous Printing” (CP), consisting in printing droplets one after the other sequentially in lines, it was used to print a continuous layer. Additive depositions were carried out on the CP pattern, depositing a layer on top of the other, up to 5 times.

Waiting time of around 15 s between each print was necessary to allow the solvent in the ink to evaporate and the print to dry.

2.3.3. Firing of half-cell

The half-cell consisting of the support, anode and electrolyte layers was subsequently fired in air. The firing consisted in a multistep debinding procedure below 700 °C for 48 h in total, to remove the organic materials for the anode and anode support substrate [24]. The simultaneous sintering of the anode and the printed electrolyte was carried out in several different conditions in single-step sintering procedures, with sintering temperature between 1000 and 1300 °C. The holding times at the sintering temperatures were 0.1, 2, and 6 h. Different holding times were used to characterize the sintering and the densification of the electrolyte.

2.3.4. Deposition of the cathode layer

Cathode ink was deposited by screen printing onto the electrolyte side of the sintered half cell (anode support/anode/electrolyte). The cathode ink was a mix of $La_{0.75}Sr_{0.25}MnO_{3-\delta}$ (LSM) and YSZ (LSM/YSZ = 50/50 vol.%). The printing speed used was 60 mm s^{-1}, the printing gap was 1 mm and the squeegee pressure was 7 bar. The printed cathode layers were then sintered at 1050 °C for 2 h. An LSM cathode contact layer was then screen printed on top of the cathode layer using the same printing described above and sintered at 1000 °C for 5 h. Further detail about the printing and the cathode specifications is described in the another paper [25].

2.4. Cell tests

2.4.1. Gas leak testing

The leak testing system used in this study works by sealing a cell of 5.3 × 5.3 cm^2 in area. The half-cells, including the sintered ink-jet printed YSZ electrolyte, were tested before cathode deposition over a manifold connected to a vacuum system. In the test, the space beneath the cell was evacuated and the pump closed off. The flow of gas into the system was measured from the rate of pressure increase, measured by a barometric gauge. The test returns a measured vacuum leak as a pressure drop slope, which was compared with a fully dense reference. Leak measurements were also carried out by monitoring the cell voltage during electrochemical single cell testing as a function of the fuel flow rate, and are described below.

2.4.2. Test fixture

The electrochemical tests were carried out using an alumina test fixture with 0.8 mm and 2.1 mm recessions on the anode and cathode side, respectively. The recessions were 40 mm wide and 40 mm long. The cathode side was contacted using a custom alumina flow-field with 19 gas channels (1 mm wide) and 20 contact ribs (1 mm wide, except the outermost ribs which were 1.5 mm wide) clad with gold strip current collectors and fine gold meshes. The anode compartment seal was made using a thin (0.08 or 0.1 mm) Au foil cut into a frame and two alumina frames were placed on top of the cells (on the cathode side) to press the cell down onto the gold seal. The anode contact component was a flat Ni-mesh resting on a Ni flow field of the same design as the cathode alumina flow-field.

2.4.3. Electrochemical measurements

The electrochemical test was performed in a FuelCon test rig. The impedance was recorded using a Solartron 1255B unit with amplitude of 60 mA (rms). The impedance data was collected from 96.9 kHz to 96.8 mHz with 12 points per decade. The cell voltage and voltage across the current shunt resistor (reference channel) were compensated (set to zero) with custom-built electronic circuitry in order to maintain maximum resolution of the Solartron unit. *I–V* curve measurements were carried out using current steps with variable step lengths and step duration of 10 s.

3. Results and discussion

Previous results on the inkjet printing of SOFC electrolytes starting from colloidal inks have shown that the probability of obtaining dense and gas-tight layers is greater when using multiple printings as compared with single-pass printings [10,15,16]. The total thickness of the printed layer depends on several factors, such as the concentration of the solid load, the particle size distribution, as well as the number of printing passes. Ink printability and wetting properties of the ink on the substrate are important to obtain a high green density of the deposited layer on the substrate [26]. Finally the sintering is crucial in the formation of the final dense layer.

3.1. YSZ-ink properties

Colloidal inks suitable for inkjet printing have to meet several key requirements [9,13]. Some important parameters associated to the solid phase in the ink are the concentration (volume fraction) of the solid, the use of a small particle size, a narrow particle size distribution, and good dispersion of the particles. Other parameters related to the ink are suitable rheological behavior, drying properties and surface tension of the liquid media. These are especially crucial to form suitable droplets upon ejection as well as to obtain stable printing with suitable wetting at the substrate [27].

For the deposition of a thin layer, nanometric powders are desirable since, when the droplet is deposited, and the ink is dried, the powders form a thin coating of packed particles, where the thickness is a result of particle size and solid concentration in the media. These two parameters are also fundamental to prevent clogging in the nozzle. Typical solid loading concentrations in colloidal inks for inkjet applications are below 10 vol.% [13]. The YSZ inks developed for this work had solid loadings of 3.7 vol.% (20 wt.%) and 0.9 vol.% (6 wt.%). The dilution in these inks was kept high with the aim to produce thin layers. Small particles are ideal for such diluted inks and small particles are usually easily dispersed in the liquid media. Nanometric YSZ powders with average particle size of ca. 50 nm were used. However, nanoparticles tend to agglomerate and to prevent this PVP was used to obtain well dispersed and stable inks [28]. A slight excess of PVP was used because an excess of a polymeric dispersant may cause some flocculation in the suspension, which tends to stabilize the ink rather than being detrimental due to the low solid loading of the ink. The resulting inks were found to exhibit excellent stability and a narrow particle size distribution. The particle size distribution for

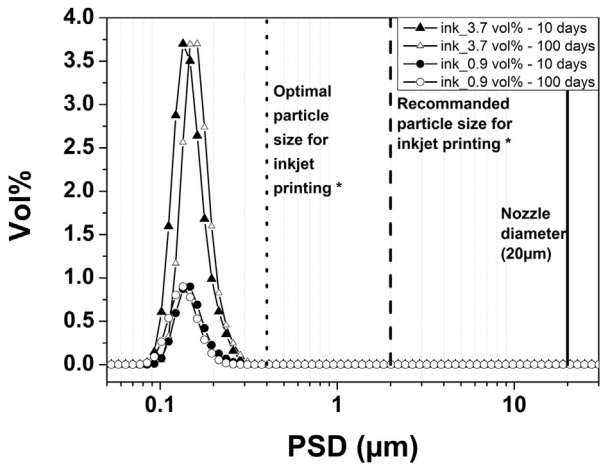

Fig. 1. Particle size distribution for the YSZ ink at low (3.7 vol.%) and high dilution (0.9 vol.%) after milling for 10 days and after 100 days of storage (* = [29]).

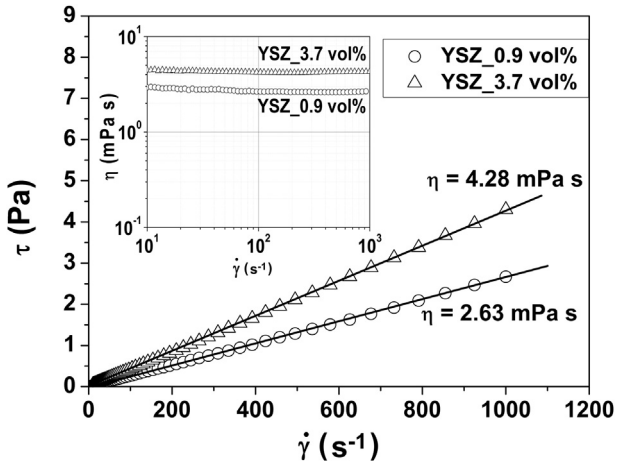

Fig. 2. Flow curves and viscosity curves (inset) for the two YSZ inks developed.

the YSZ-inks was measured immediately after preparation, after 10 days of milling and, in order to estimate the long term stability, after 100 days of storage without agitation. Fig. 1 shows the typical particle size distribution within the range of 0.06 and 0.34 μm with a max at around 100 nm. Such nanometric powders exhibited high stability with no precipitation and preserving the same distribution even after 100 days of storage. Moreover, to avoid clogging of the print head nozzle the particle size should preferably be less than 10% of the nozzle diameter, while the optimal value has been estimated to be around 2% [29]. The HP-Deskjet 1000 has a nozzle diameter of around 20 μm diameter which for a maximum particle size of 0.34 μm corresponds to (0.34 μm/20 μm) = 1.7%.

The rheology of the inks was characterized using dynamic conditions. Fig. 2 shows the flow curves for the two inks with the correspondent viscosity curves (the inset). Both inks exhibit Newtonian behavior with a constant viscosity independent of the shear rate (inset). The viscosity values were calculated from the slope of the flow curves. The values obtained were 4.28 mPa s for the 3.7 vol.% ink and 2.63 mPa s for the 0.9 vol.% ink.

These values are usually considered suitable for a thermal DoD inkjet system [13]. The surface tension of the ink was measured using a bubble pressure tensiometer and yielded a value of 36 mN m^{-1}.

A range of the parameters, *Z*, *We*, and *Re* numbers (defined in Experimental section) yielding optimal printability of inks has been identified in literature. For *Z*, Jang et al. [30] proposed a range between 4 and 14, whereas Derby et al. [31] suggested a value for *Z*

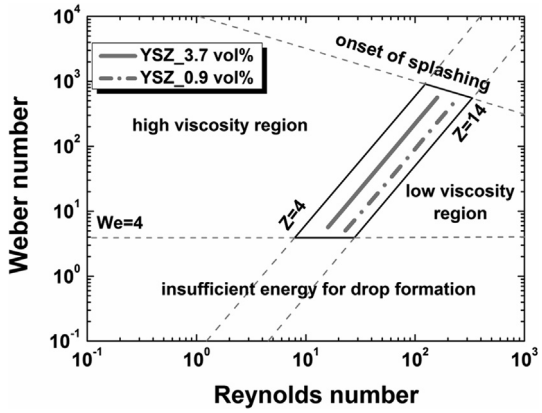

Fig. 3. Weber–Reynolds numbers diagram defining the regime for ink properties which ensure good printing characteristics. This diagram has been proposed by Derby [27].

Table 1
Ink properties.

Ink	Vol.%	η (mPa s)	σ (mN m^{-1})	ρ (g cm^{-3})	*Z*
20 wt.%	3.7	4.28	36.4	1.14	6.73
6 wt.%	0.9	2.63	36.2	1.01	10.28

between 1 and 10. Moreover, Derby proposed the *We*–*Re* numbers diagram to illustrate the regime of printability for the ink properties. Such a diagram is displayed in Fig. 3 and shows that the *We* and *Re* values calculated for the two developed inks are within the identified printability region. The properties of the developed inks are summarized in Table 1.

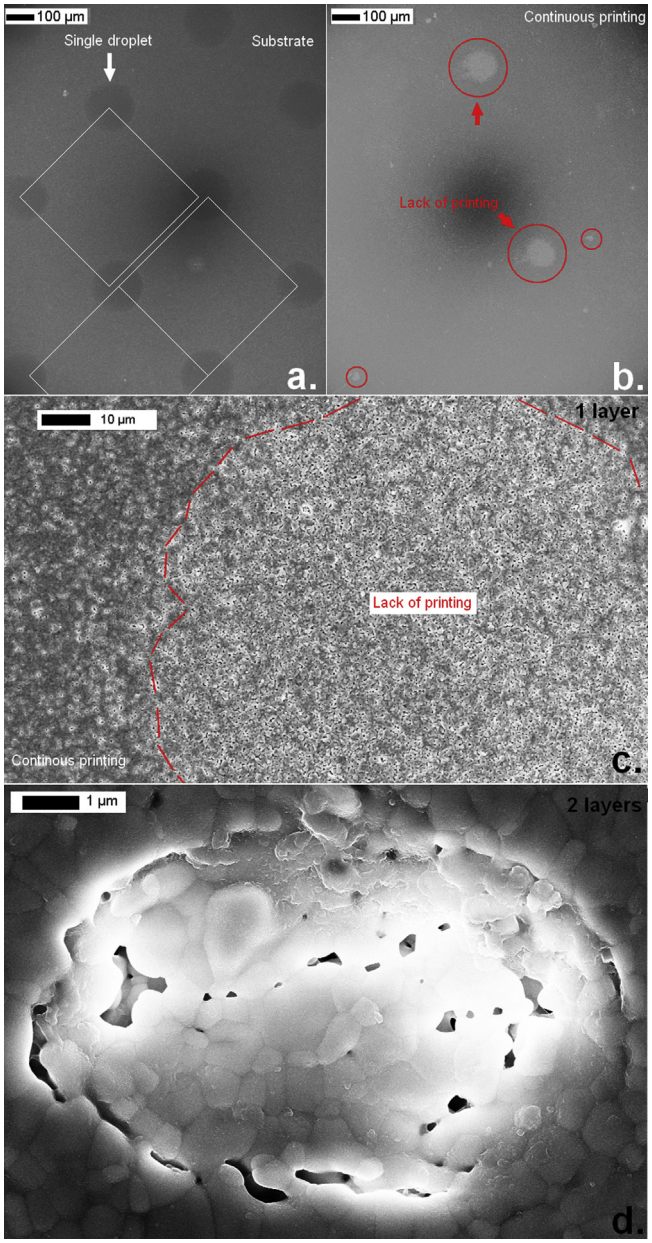

Fig. 4. SEM observations of the YSZ printings, after sintering at 1300 °C for 5 min. (a) 0.9 vol.% ink printed as single droplets, (b) continuous print using the 3.7 vol.% ink, (c) high magnification of printing flaw shown in (b), (d) typical defect on a two layer deposition.

3.2. Inkjet printing and sintering of the YSZ electrolyte

The use of a low-cost inkjet process for the fabrication of a continuous layer leads to formation of some critical flaws. Particularly, since each single layer is formed drop by drop, any alignment errors and/or lack of deposition (missing drops) during the printing create discontinuity in the layer. Moreover, extremely dilute inks can lead to poor packing of the particles, leaving residual porosity and presence of pinholes in the sintered layer. Fig. 4a–d shows the typical flaws observed by SEM after printing of the diluted YSZ inks; Fig. 4a shows the typical alignment of the droplets obtained by inkjet of the highly diluted ink (0.9 vol.% of YSZ loading) after sintering at 1300 °C for 6 h. The alignment is crucial for the formation of a continuous single layer, where all the droplets forming the continuous layer have to be placed in the desired positions. The SEM observations on the layers produced using single droplet printing (SD) indicated that, although the droplets were designed in an ordered pattern, a certain misalignment in the range of few micrometers occurred for some of the droplets (see white squares superimposed in Fig. 4a). This effect is possibly associated with the lack of precision in the mechanical movement system. Fig. 4b shows the results of continuous printing (CP) of a single layer of the concentrated (low dilution) ink. This showed evidence of missing droplets in several areas of various sizes and shapes. Particularly, several large circular regions of around 100 μm in diameter were observed. In these cases, the size was similar to the droplets formed by SD and the lack of printing is probably caused by an imprecise impact of the droplets on the substrate or a defective droplet formation at the nozzle. Other small defects with irregular shapes were also observed in the CP (see red (in the web version) circles in Fig. 4b) and are attributed to the presence of imperfections at the substrate surface, which may impair the settling of the particles after printing. A closer look at the circular flaw after sintering at 1300 °C for 6 h is shown in Fig. 4c. In this figure the bright area corresponds to the slightly porous surface of the substrate and red (in the web version) lines are superimposed to highlight the edges of the defect. Presence of porosity around the edge could be observed, suggesting an excessive dilution of the ink at the boundary between the drops. On the other hand, all the covered areas showed homogeneity and a high degree of packing of the particles which led to densification of the layer after sintering at 1300 °C. It is also worth noticing that no coffee-stain rings or other particle agglomeration effects were detected in the samples. This observation confirms the suitable printing characteristics of the developed inks. However, the presence of the several defects detected at the CP single layer highlights the need for using a multiple-printing approach to fabricate a gas-tight electrolyte with the present printing technology. Fig. 4d shows a typical SEM image of the 2-layer deposition by the 3.7 vol.% ink after sintering at 1300 °C for 6 h. Particularly, the picture shows the filling-in of a small defect in the first layer by the second print-pass. The particles in the flaws exhibited sintering with presence of residual porosity. This effect can possibly be attributed to an excessive dilution on the solid, where the low concentrations of the material can only partially cover the defect. This effect generated porosity and resulted in a discontinuous layer. Increasing the number of print-passes (depositions) should minimize this issue.

Fig. 5a–e shows SEM images of the printed electrolyte using the 3.7 vol.% ink exposed to various sintering profiles. Fig. 5a–c shows the particles sintered at 1000 °C, 1150 °C and 1300 °C for 6 min. The short dwelling time used made it possible to follow the evolution of the microstructure primarily as function of the temperature. Fig. 5a shows that, at 1000 °C, the YSZ particles in the deposit are of a round shape and with a homogenous size of ca. 100 nm. The packing is rather high with no agglomeration. However, large voids among the particles, probably formed during the ink drying process, were observed. Fig. 5b shows that at 1150 °C the YSZ particles are connected by the typical necking, indicating an incipient sintering at the layer with formation of small and larger porosity (below 1 μm), where the latter probably was due to the voids as shown in Fig. 5a. The result after sintering at 1300 °C is shown in

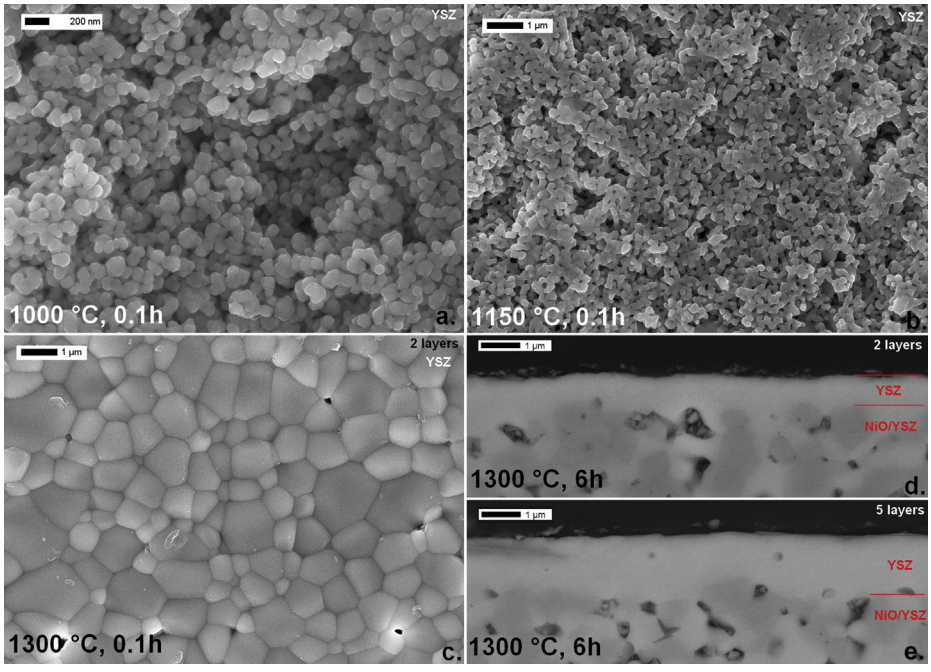

Fig. 5. SEM observations of the YSZ printings by the 3.7 vol.% ink. (a) continuous printing sintered at 1000 °C for 6 min, (b) 1150 °C for 6 min, (c) 1300 °C for 6 min, and the cross-section pictures of the half cells made by of (d) 2-layer and (e) 5-layer depositions after sintering at 1300 °C for 6 h.

Table 2
Leak test results and thickness measurements of 2-layer and 5-layer electrolyte half cells.

Sample	Number of printed layers	Sintering conditions	Reference pressure slope (mbar s^{-1})	Measured pressure slope (mbar s^{-1})	Electrolyte thickness (μm)
2-Layer	2	1300 °C/6 h	0.46	0.46	0.6
5-Layer	5	1300 °C/6 h	0.46	0.08	1.2

Fig. 5c. The figure clearly shows that the treatment led to a full densification and grain growth. The original particle grew to the micrometer range and the resulting layer was rather dense with annihilation of all the porosity, including the voids in Fig. 5b.

In conclusion the 3.7 vol.% ink is proven to be suitable for the formation of continuous YSZ layers and a sintering temperature around 1300 °C can be used for the densification. However, as discussed above, printing defects suggest that multiple printing with more than 2-layers should be used to avoid pinholes in large-area cells. Fig. 5d and e shows the cross-section at the half cells, after sintering at 1300 °C for 6 h, for 2-layer and 5-layer depositions using the 3.7 vol.% ink. Both the layers resulted dense and homogenous and typical thickness of *app.* 0.6 μm and 1.2 μm were estimated for the 2-layer and the 5-layer samples, respectively. The relation between the thickness and number of depositions/print-passes was found to be non-linear and this was attributed to heterogeneous roughness of the substrate surface and to the lack of deposition of the continuous printing.

To further characterize the tightness of the printed layers leak tests were carried out with the sintered 5 × 5 cm^2 half cells. Table 2 shows that leak test performed on the 2-layer electrolyte exhibits a measured pressure slope value similar to the reference pressure slope, indicating insufficient electrolyte gas tightness. The pressure slope measured with the 5-layer electrolyte was very low compared to the reference (sheet of steel), indicating a high tightness of the electrolyte.

3.3. Cell performance

Two SOFCs with a 2-layer and a 5-layer electrolyte, respectively, were manufactured with a 4 × 4 cm^2 active area (defined by the cathode) as described in the Experimental section. The cell produced with the 2-layer electrolyte was not leak tight and open circuit voltages of less than 0.7 V were observed in dilute (9%) hydrogen. Moreover, the electrolyte gas tightness decreased rapidly during the test, most likely due to re-oxidation of the Ni-cermet anode. This is in agreement with the ex-situ leak testing that was carried out and reported in the previous section. The cell with the 5-layer electrolyte was significantly more leak tight. Open circuit cell voltages in the range 1.07–1.15 V were observed in dry hydrogen fuel at flow rates in the range 6.7–31.7 ml min^{-1} cm^{-2}, as can be seen in Fig. 6. The leak was quantified by calculation of a total leak current, a measure of the total leak, both external (e.g. through seals and anode support) and internal (electrolyte pinholes, cracks), using the relations derived by Rasmussen et al. [32]. No systematic variation of the leak current with the fuel flow was observed, indicating the absence of large cracks or holes in the cell or the sealing gasket used on the anode side.

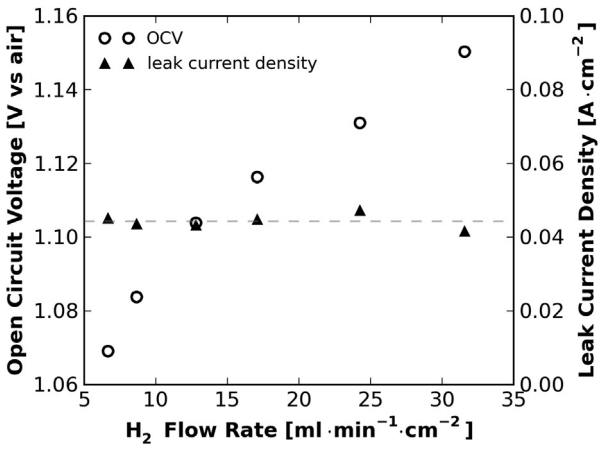

Fig. 6. Observed open circuit cell voltage (open circles) and calculated total leak current density (according to Rasmussen et al., filled triangles) of 5-layer electrolyte SOFC operates with dry hydrogen supplied as the fuel at the indicated flow rates and air as the oxidant. The dotted horizontal line represents the average leak current density (0.044 A cm^{-2}), calculated using the active area of the cell (=16 cm^2).

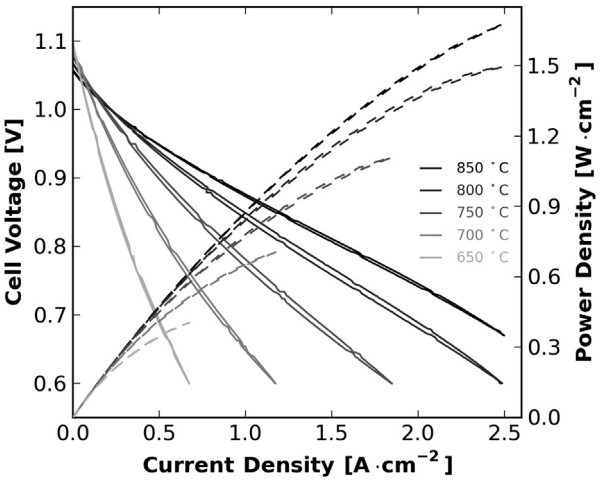

Fig. 7. Polarization curves recorded for the 5-layer electrolyte SOFC (active area = 16 cm^2) which was tested with a composite LSM–YSZ cathode and an LSM current collection layer. The fuel was 96% H_2 and 4% H_2O supplied at a total flow rate of 26 ml min^{-1} cm^{-2}. The lower voltage limit was set to 0.6 V and the maximum current limit to 2.5 A cm^{-2} (40 A).

Polarization curves were recorded at operating temperatures in the range from 850 °C down to 650 °C with 50 °C increments. Fig. 7 shows polarization and power curves for the 5-layer electrolyte SOFC. At 750 °C the area specific secant resistance was 0.26 Ω cm^2 (0.21 Ω cm^2 after correction for fuel utilization) and the observed power density at 0.6 V was 1.2 W cm^{-2} [33].

The theoretical area specific resistance contribution from a 1.2 μm thick 8YSZ layer is 0.004 Ω cm^2 at 750 °C based on bulk

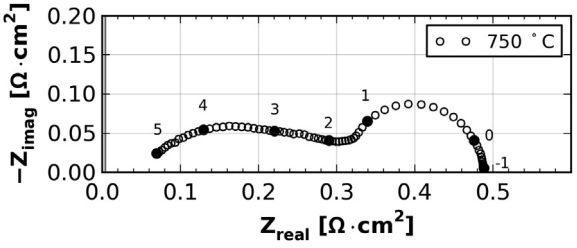

Fig. 8. Nyquist plot of the electrochemical impedance spectrum recorded with the 5-layer electrolyte SOFC at 750 °C and with 96% H_2 + 4% H_2O as the fuel and air as the oxidant. The impedance data was collected with 12 points per decade, indicated in the figure by filled symbols (also marked with the logarithm of the frequency), starting at 96.9 kHz (at low Z_{real} values). The dashed gray line indicates the theoretical resistance of the 1.2 μm thick 8YSZ electrolyte based on bulk conduction properties. The data in the plot was corrected for lead inductance.

conductivity data for 8YSZ [34]. An ohmic resistance of approximately 0.05–0.06 Ω cm^2 was observed at 750 °C (see Fig. 8). This is more than ten times greater than the theoretical resistance expected from the electrolyte layer in the tested cell, but on the other hand a quite similar offset of 50–60 mΩ cm^2 is often seen and has previously been reported with a 10 μm thick ink-jet printed YSZ electrolyte [35]. Additionally, the cathode deposition method was reported to affect the series resistance [35]. Explanations to the observed high series resistance could be limited measurement range (the maximum frequency was 96.5 kHz). Other contributions to the observed ohmic resistance could be imperfect contacting of the electrolyte by the cathode layer, current constriction, or secondary phases formed at the interface [36]. Significant current collection losses are deemed unlikely as a sufficiently conducting current collection layer was used.

The ohmic resistance observed in electrochemical impedance spectroscopy can be assigned to the electrolyte, if it is measured to sufficiently high frequency, and assuming that there are no additional contributions to the ohmic resistance from current collection and the porous composite electrodes. Sufficient conductivity in the cathode current collection layer was confirmed by in-plane van der Pauw conductivity measurements [37]. Even though the observed ohmic resistance was much higher than the theoretical value, most of the impedance of this cell is related to the electrodes, and by improving the electrodes and ensuring a better contact to the electrolyte, a significant reduction in both ohmic and polarization resistance can be expected. This highlights the potential performance gain of cells with thin electrolyte, and further supports the feasibility of ink-jet based printing techniques for production of solid oxide cell components.

4. Conclusions

A 1.2 μm SOFC YSZ electrolyte was successfully fabricated by inkjet printing using a low-cost HP Deskjet 1000 DoD inkjet printer and an optimized 3.7 vol.% YSZ colloidal water-based ink. Missing droplets and imprecise impact on the anode substrate was observed to produce areas with lack of deposition when printing single layers. Inks with high dilution and nanometric particles improve printability and stability, however printing of multiple layers seems necessary to cover the defects formed during single layer printing. 2 layers were insufficient, but 5 layers resulted in a gas tight electrolyte. Although the electrolyte resistance was higher than expected from calculations using known bulk-electrolyte resistance, an SOFC tested with the electrolyte, an LSM/YSZ cathode and a Ni/YSZ anode produced an OCV above 1.15 V and a power peak density of 1.5 W cm^{-2} at 800 °C.

Acknowledgments

The authors gratefully acknowledge support from Energinet.dk through the ForskEL programme (project # 2012-1-10747).

References

[1] H. Minemawari, T. Yamada, H. Matsui, J. Tsutsumi, S. Haas, R. Chiba, R. Kumai, T. Hasegawa, Nature 475 (2011) 364–367.
[2] T. Wang, B. Derby, J. Am. Ceram. Soc. 88 (2005) 2053–2058.
[3] H. Sirringhaus, T. Kawase, R.H. Friend, T. Shimoda, M. Inbasekaran, W. Wu, E.P. Woo, Science 290 (2000) 2123–2126.
[4] M. Singh, H.M. Haverinen, P. Dhagat, G.E. Jabbour, Adv. Mater. 22 (2010) 673–685.
[5] D. Tobjörk, R. Österbacka, Adv. Mater. 23 (2011) 1935–1961.
[6] A.D. Taylor, E.Y. Kim, V.P. Humes, J. Kizuka, L.T. Thompson, J. Power Sources 171 (2007) 101–106.
[7] J. Ebert, E. Ozkol, A. Zeichner, K. Uibel, O. Weiss, U. Koops, R. Telle, H. Fischer, J. Dent. Res. 88 (2009) 673–676.
[8] R.L. Kenion, W.Y. Lee, in: 2011 IEEE 37th Annu. Northeast Bioeng. Conf, 2011, pp. 1–2.
[9] G.D. Martin, S.D. Hoath, I.M. Hutchings, J. Phys. Conf. Ser. 105 (2008) 012001, 1–14.
[10] R.I. Tomov, M. Krauz, J. Jewulski, S.C. Hopkins, J.R. Kluczowski, D.M. Glowacka, B.A. Glowacki, J. Power Sources 195 (2010) 7160–7167.
[11] I. Van Driessche, S. Hopkins, P. Lommens, X. Granados, D. Andreouli, B. Glowacki, I.M. Arabatzis, M. Arin, S. Ricart, I. Fasaki, E. Georgiopoulos, R. Tomov, Nanosci. Nanotechnol. Lett. 5 (2013) 466–474.
[12] D. Young, A.M. Sukeshini, R. Cummins, H. Xiao, M. Rottmayer, T. Reitz, J. Power Sources 184 (2008) 191–196.
[13] H. Kipphan, in: H. Kipphan (Ed.), Handbook of Print Media, Springer-Verlag, Berlin, Heidelberg, New York, 2001, pp. 711–730.
[14] J. Will, A. Mitterdorfer, C. Kleinlogel, D. Perednis, L.J. Gauckler, Solid State Ionics 131 (2000) 79–96.
[15] C. Wang, R.I. Tomov, R. Vasant Kumar, B.A. Glowacki, J. Mater. Sci. 46 (2011) 6889–6896.
[16] C. Li, H. Shi, R. Ran, C. Su, Z. Shao, Int. J. Hydrogen Energy 38 (2013) 9310–9319.
[17] A. Weber, E. Ivers-Tiffée, J. Power Sources 127 (2004) 273–283.
[18] X. Xin, Z. Lü, X. Huang, X. Sha, Y. Zhang, W. Su, Mater. Res. Bull. 41 (2006) 1319–1329.
[19] X. Chen, K. Khor, S. Chan, L. Yu, Mater. Sci. Eng. A 335 (2002) 246–252.
[20] S.P. Jiang, S.H. Chan, J. Mater. Sci. 39 (2004) 4405–4439.
[21] F. Teocoli, D.W. Ni, K. Brodersen, S.P.V. Foghmoes, S. Ramousse, V. Esposito, J. Mater. Sci. 49 (2014) 5324–5333.
[22] A.L. Yarin, Annu. Rev. Fluid Mech. 38 (2006) 159–192.
[23] A. Hauch, M. Mogensen, Solid State Ionics 181 (2010) 745–753.
[24] J. Glasscock, V. Esposito, S.P.V. Foghmoes, T. Stegk, D. Matuschek, M.W.H. Ley, S. Ramousse, J. Eur. Ceram. Soc. 33 (2013) 1289–1296.
[25] M.J. Jørgensen, M. Mogensen, J. Electrochem. Soc. 148 (2001) A433–A442.
[26] J. Wang, J. Evans, Phys. Rev. E 73 (2006) 021501, 1–8.
[27] B. Derby, Annu. Rev. Mater. Res. 40 (2010) 395–414.
[28] D. Marani, J. Hjelm, M. Wandel, J. Eur. Ceram. Soc. 34 (2014) 695–702.
[29] I.M. Hutchings, in: I.M. Hutchings, G.D. Martin (Eds.), Inkjet Technology for Digital Fabrication, Wiley, 2013, pp. 1991–1994.
[30] D. Jang, D. Kim, J. Moon, Langmuir 25 (2009) 2629–2635.
[31] B. Derby, N. Reis, MRS Bull. (2003) 815–818.
[32] J.F.B. Rasmussen, P.V. Hendriksen, A. Hagen, Fuel Cells 8 (2008) 385–393.
[33] M. Mogensen, P.V. Hendriksen, in: S. Singhal, K. Kendals (Eds.), High Temp. Solid Oxide Fuel Cells, Elsevier Science, 2003, pp. 261–289.
[34] C.C. Appel, N. Bonanos, A. Horsewell, S. Linderoth, D. Roskilde, J. Mater. Sci. 6 (2001) 4493–4501.
[35] M. Sukeshini, R. Cummins, T.L. Reitz, R.M. Miller, J. Am. Ceram. Soc. 92 (2009) 2913–2919.
[36] D.Z. de Florio, R. Muccillo, V. Esposito, E. Di Bartolomeo, E. Traversa, J. Electrochem. Soc. 152 (2005) A88–A92.
[37] M. Van der Pauw, Philips Res. Reports 13 (1958) 1–9.